Application of Inverted Slope Images for Geological Mapping – Reduction of Artifacts in Digital Elevation Models by Filtering in the Frequency Domain

Yajima, T.[1, 2] and Yamaguchi, Y.[2]
[1]Japan Oil, Gas and Metals National Corporation (JOGMEC), Toranomon 2-10-1, Minato-ku, Tokyo, Japan, 105-0001, E-mail: yajima-taro@jogmec.go.jp
[2]Nagoya University, Graduate School of Environmental Studies, D2-1 (510) Furo-cho, Chikusa-ku, Nagoya, Japan, 464-8601, E-mail: yasushi@nagoya-u.ac.jp

Abstract
Inverted slope images created from digital elevation models (DEMs) can be used to visualize differences in lithological units and provide an indication of areas of geological outcropping. Such images are useful for geological mapping, but when created from DEMs generated from remote sensing images ("image-derived DEMs"), artifacts in the DEMs are exaggerated and give rise to unclear noisy final images. Such artifacts also affect the quality of normal slope images and shaded relief images. In contrast, DEMs created from elevation data in the form of contour maps ("contour-derived DEMs") contain far fewer artifacts, but their availability is limited. Therefore, in order to obtain clear processed DEM images that can be used for global geological mapping, it is necessary to develop a method for reducing the number of artifacts in image-derived DEMs. In the present study, the effectiveness of a fast Fourier transform (FFT) for artifact reduction in image-derived DEMs was investigated. The FFT converts spatial data into the frequency domain, and artifacts with specific frequencies are removed by low-pass filtering. An inverse FFT is then used to return to the spatial domain, thus producing a filtered DEM with a reduced number of artifacts. The effect of the filter size on the final image quality was also investigated. The image-derived DEMs used in this study were the Shuttle Radar Topography Mission (SRTM) DEM and the Advanced Spaceborne Thermal Emission and Reflection Radiometer (ASTER) Global DEM (GDEM) for Cuprite, Nevada. A comparison was made between shaded relief and inverted slope images created following artifact removal from these DEMs and equivalent images produced using the contour-derived National Elevation Dataset (NED) DEMs. It was clarified that for the image-derived DEMs, that a low-pass filter with a size of 20 to 40 % significantly reduced the number of artifacts without significant loss of terrain information. For the ASTER GDEM data, artifact reduction was found to be particularly important because the artifacts obscure the original topographic information in the inverted slope images.

1. Introduction

Compared to other forms of remote sensing data, digital elevation models (DEMs) have not been used extensively for geological mapping. Rather, geological mapping has typically been performed using color composite images produced from multi-band sensor platforms, such as Landsat (Crosta and Moore, 1989) and Advanced Spaceborne Thermal Emission and Reflection Radiometer (ASTER) data (Hewson et al., 2005). However, DEMs have been used as subsidiary data to clarify linear or circular relief patterns for tectonic and structural analysis in geology (Masoud and Koike, 2006). Recently, studies using DEMs have increased, and DEMs have been used for landform mapping (Smith and Clark, 2005) and terrain classification (Iwahashi and Pike, 2007). DEM images that have been processed to show shaded relief and aspect have been used for geological mapping (Badura and Przybylski, 2005, Singh and Dowerah, 2010). In this paper, we describe the application of inverted slope images created from DEM images for geological mapping, and also propose a method to reduce artifacts from image-derived DEMs. A variety of spatial filtering (Brown and Bara, 1994) and frequency filtering (Hassan, 1988 and Pan, 1989) methods have been developed to reduce the number of artifacts that are generated when DEMs are produced from contour lines. DEMs derived from remote sensing image data, such as the data collected by the Shuttle Radar Topography Mission (SRTM) (Rabus et al., 2003 and Gesch et al., 2006) and Global DEM (GDEM) of the Advanced Spaceborne Thermal Emission and Reflection Radiometer (ASTER) (Fujisada et al., 2005 and Tachikawa et al., 2011), currently almost cover the entire earth, and use of these image-

derived DEMs currently exceeds that of contour-derived DEMs. Although contour- and image-derived DEMs have similar topography data, the processed DEM images, such as images with shaded relief and inverted slope images obtained from image-derived DEMs, are considerably noisier than those obtained from contour-derived DEMs. Consequently, reducing the artifacts in image-derived DEMs needs to be achieved in order to increase the potential application of image-derived DEMs, such as SRTM DEM and ASTER GDEM, to geological mapping.

2. Contour- and Image-Derived DEMs

A DEM is an ordered array of ground elevations at regularly spaced intervals. DEM data is originally point data consisting of latitude, longitude and altitude, but normally gridded to raster data. According to Guth (1999), DEMs can be divided into two groups depending on whether the source of data used to generate the DEM is (1) contour lines ("contour-derived DEM"), or (2) remote sensing imagery ("image-derived DEM"). Contour-derived DEMs are created from hypsographic maps produced by aerial photogrammetry and triangulation surveys. The height information in a contour-derived DEM is ground elevation data. Examples of contour-derived DEMs include the National Elevation Dataset (NED) of the United States, Canadian Digital Elevation Data (CDED), and the Japan Profile for Geographic Information Standards (JPGIS). Relatively few countries have accurate contour maps for public use and the availability of contour-derived DEMs is limited. Image-derived DEMs are generated using remote sensing imagery and are not correlated with direct ground data. The height information in image-derived DEMs is canopy elevation. SRTM DEM and ASTER GDEM are typical image-derived DEMs with a near global coverage and are freely available. NED DEM (a contour-derived DEM), and SRTM DEM and ASTER GDEM (image-derived DEMs) were used and compared in this study. Features of each DEM-type are shown in Table 1.

3. Study Area

Cuprite in southwestern Nevada, approximately 200 km northwest of Las Vegas, was selected as the study area for geological mapping as the outcrop conditions are well and the geology, with its diverse hydrothermal alteration mineralogy, is well defined. Cuprite has been used extensively as a test site for a variety of remote sensing studies; particularly for extensive alteration mineral mapping exercises using AVIRIS data (Kruse, 2002), ASTER data (Rowan et al., 2003), Hyperion data (Kruse et al., 2003) have been conducted. The regional geology of the Cuprite area has been described by Crafford (2007). Briefly, the area is composed of Lower Cambrian to Latest Proterozoic clastic rocks consisting of cross-bedded quartzite, siltstone, and phyllite (Czq) are underlain by Cambrian sedimentary units consisting of phyllite, schist, shale, thin-bedded limestone, chert, and siltstone (Ctd), which create the high northeast- to southwest-trending ridges that characterize the study area. Tertiary volcanic and sedimentary rocks, such as intermediate silicic ash flow tuff (Tt2), younger rhyolitic flows, and shallow intrusive rocks (Tr3), younger silicic ash flow tuffs (Tt3), and younger tuffaceous sedimentary rocks (Ts3) are present over the lower sedimentary rocks and create gentle hills. Quaternary sediments, such as playa and floodplain deposits (Qpl) and alluvium (Qal) are present and cover the flat terrain (Figure 1).

4. Inverted Slope Images for Geological Mapping

A slope image is created using the steepest neighbor algorithm which is the maximum rate of change in value from the center to its neighbor cells (Guth, 1995). It is an approximate derivative of the original DEM. Gradient values in the slope image can be expressed in percent or degree units. The use of other algorithms, such as four or eight closest neighbors would change the values slightly, but would not change the resulting patterns. For shaded relief images, sun illumination is from one direction only and some surface features are hidden by this orientation-effect.

Table 1: Contour-derived DEM and image-derived DEM used for the study

	NED	SRTM (SRTM1)	ASTER GDEM (GDEM2)
DEM type	Contour-derived DEM	Image-derived DEM	Image-derived DEM
Data provider country	USA	USA	Japan
Horizontal grid spacing	1 arc second	1 arc second	1 arc second
Coverage	Contiguous US, Hawaii and Puerto Rico (Except for Alaska)	Contiguous US, Hawaii and Puerto Rico (Alaska to 60°N)	83°N to 83°S
Data source	Aerial photos	C-band SAR	ASTER VNIR band3N/B
DEM production	Contour to grid	Interferometry	Stereography

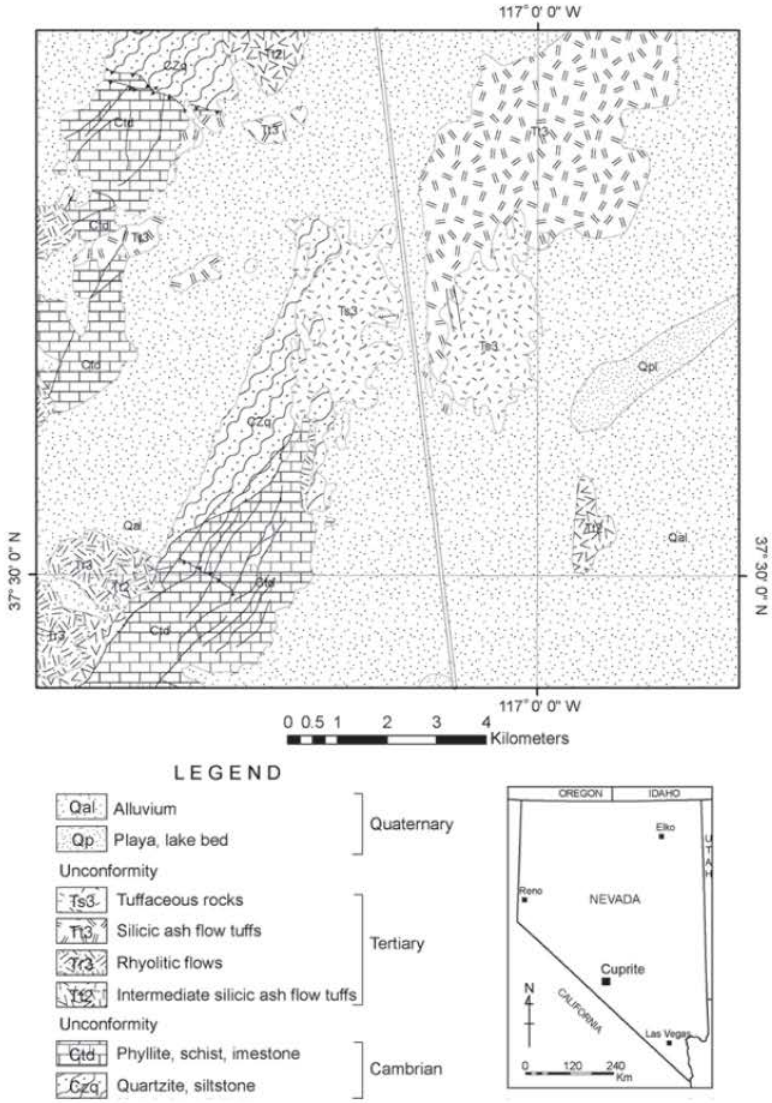

Figure 1: Geological map of the study area (modified after Crafford, 2007).

The flanks of Stonewall Mountain in the southeast of the study area are invisible in the shaded relief images because the direction of sun illumination is from the southeast (Figure 2 (a), (b), (c)). There is no orientation dependence in the slope images (Figure 2 (d), (e), (f)), but the lithology of the original slope image is difficult to interpret because the image is dark and the contrast is low. Consequently, detail of the topographic features was enhanced by inverting the slope image (Figure 2 (g), (h), (i)) to display the lithological units in a different tone and texture with stronger contrast. In these inverted images, dark tones indicate outcrop areas with rigid terrain consisting of lithological units that are typically hard and resistant to weathering. White areas indicate flat or gently sloping terrain, such as talus areas covered by overburden and free of any outcrops. The inverted slope images provided considerable information on the distribution of lithological units. The clearest inverted slope image was obtained from contour-derived NED DEM data, while that obtained from GDEM data was extremely noisy.

5. DEM Artifacts

Artifacts in the image-derived DEMs are both exaggerated and visible in the shaded relief and inverted slope images. Three types of artifacts were observed in the images used in this study (Figure 2, Figure 3).

1) Anomalous topographic features in the shaded-relief and slope images derived from the ASTER GDEM data in the eastern part of the study area

(Figure 2 (c), (f), (i)). These anomalous features in the ASTER GDEM data were observed in areas with low ASTER scene stack numbers, i.e., in areas with relatively few cloud-free images.

2) Fine-grained noise was extensive in the inverted slope images derived from SRTM DEM and ASTER GDEM data (Figure 2 (h), (i)). The random noise observed in the ASTER GDEM inverted slope image was more intense than that observed in the SRTM DEM data, and the noise obscured topographic information.

However, these random artifacts were uniformly present in the SRTM DEM and ASTER GDEM data (Figure 3 (b), (c)). In addition, the magnitude of the random noise was small in the topographic section, but markedly higher in the slope sections (Figure 3 (e), (f)).

3) Single-point spike-type errors were observed in the topographic sections of the ASTER GDEM data (Figure 3 (c)); these errors are typically difficult to perceive in both shaded-relief images and inverted slope images (Figure 3 (c), (f)).

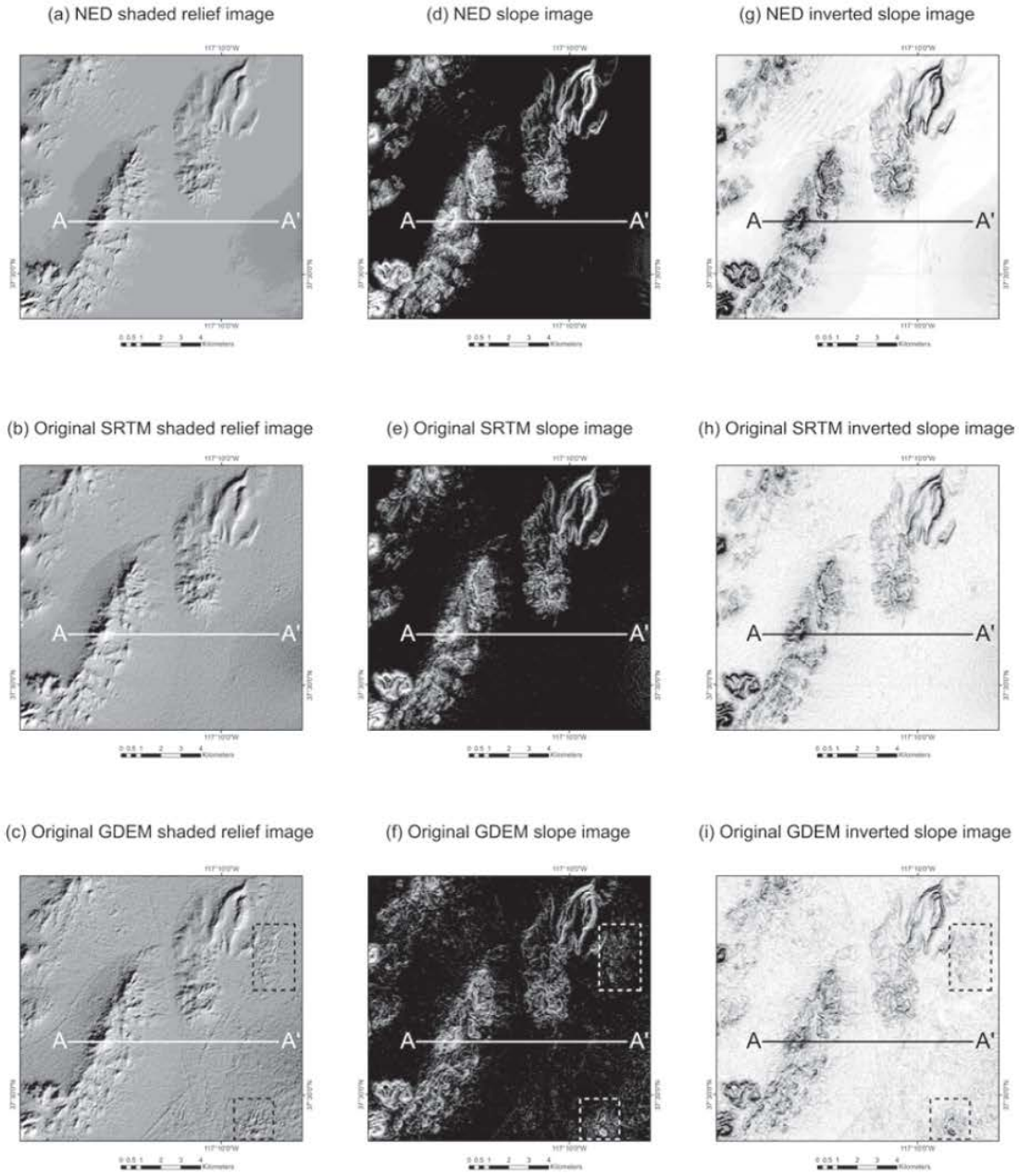

Figure 2: Shaded relief images, slope images and inverted slope images of the study area

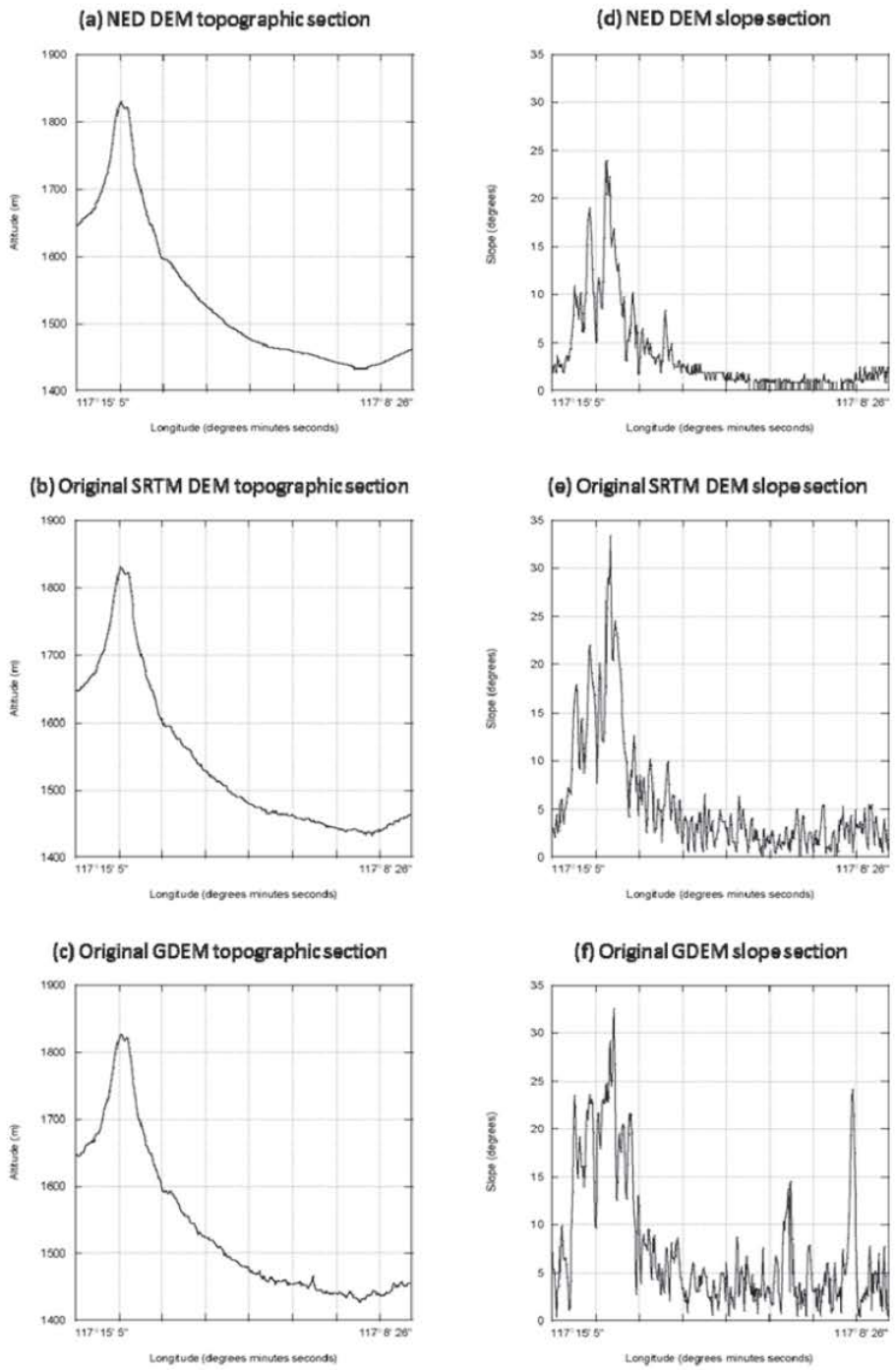

Figure 3 DEM topographic sections and DEM slope sections of line A-A' in figure 2

Contour-derived NED DEM images had fewer artifacts compared to the image-derived DEM images, but they were not completely free of artifacts. For example, artifacts referred to as contour "ghosts" were observed in imagery of the northwestern part of the study area in both the shaded-relief and inverted slope images (Figure 2 (a), (d), (g)). Contour "ghosts" are associated with the contour to grid algorithm producing grid-node elevations with the same elevation (Guth, 1999). They are small artifacts and do not appear as elevation errors in the topographic and slope sections. Collection line artifacts, which produce stripes or aligned textures in USGS 7.5 minute DEM data, have been reported (Albani and Klinkenberg, 2003), but no such artifacts were

observed in this study area. Image-derived DEM data contains more artifacts than the contour-derived DEMs generally. Reducing artifacts from image-derived DEMs is therefore considered important for obtaining smooth topographic information. Although SRTM DEM and ASTER GDEM both contain artifacts that can be attributed to topographic information, it is clear that ASTER GDEM contains more artifacts than SRTM DEM.

6. Artifact Reduction Methods

Spatial filters are effective for reducing spike-type errors in a DEM, but if spatial filtering is applied to an entire DEM, it will decrease the spatial resolution and diminish the detailed features of all of the original DEM information. The application of spatial filters should therefore be restricted to spike-type artifacts. When using multiband remote sensing data, valid elevation information can be distinguished from artifacts by performing a principal components analysis (PCA) or maximum noise fraction (MNF) transformation (Green et al., 1988), which will separate information and artifacts into different PCA clusters (Crosta and Moore, 1989 and Loughlin, 1991) or MNF bands (Kruse et al., 2003). Artifact reduction can then be achieved by deleting those bands dominated by noise, and then reverting back to the PCA or MNF data; however, PCA and MNF analyses cannot be applied to single band data.

Fast Fourier transformation (FFT) can reduce artifacts from single band data and FFT has been employed to reduce systematic artifacts from remote sensing images (e.g., de Souza Filho et al., 1996). Figure 4 shows a flow chart describing the process for reducing artifacts from DEMs. Briefly, spatial data is transformed into the frequency domain by FFT.

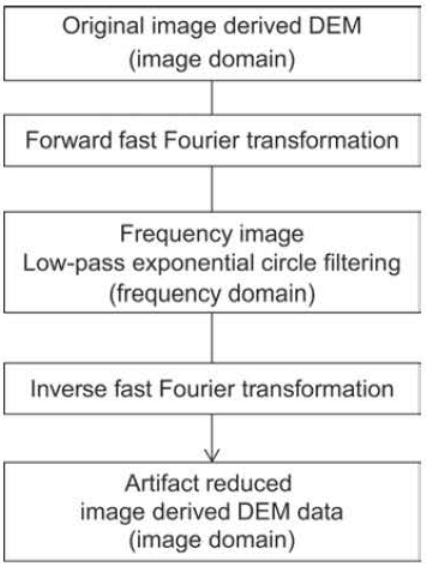

Figure 4: Flow chart for reducing artifacts from DEM data

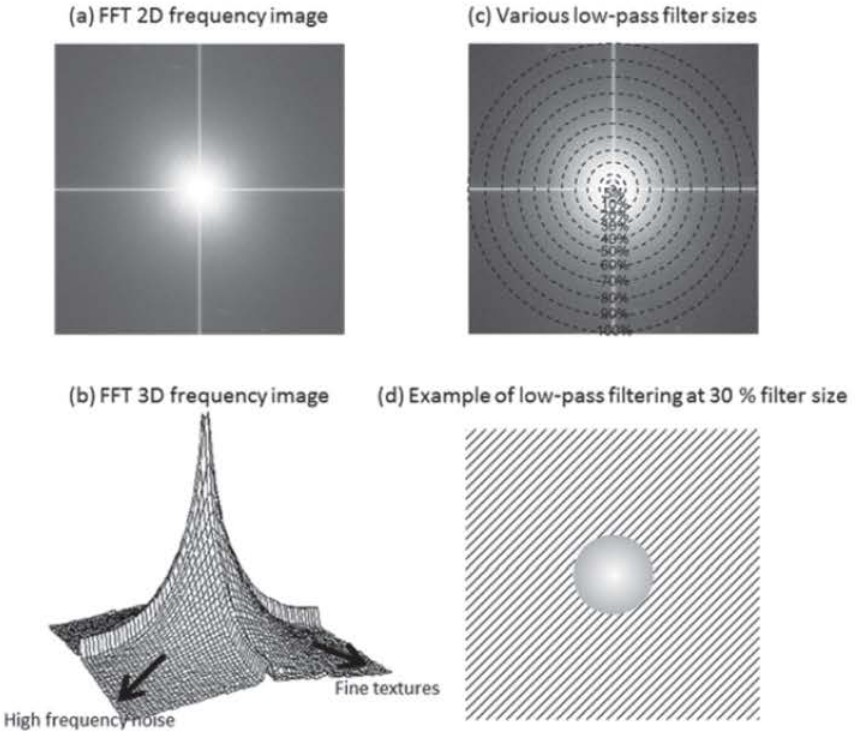

Figure 5: FFT frequency images and low-pass filter sizes

Intrinsic image and elevation information is concentrated at low frequencies which are located at the center of the FFT frequency image (Figure 5 (a)) creating a peak and troughs representing the high frequency information which contains very fine textured information and noise (Figure 5 (b)). Specific high-frequency artifacts in the image-derived DEMs can then be removed by applying a low-pass filter of a specific size to the FFT frequency data (Figure 5 (c)). After filtering the high frequency components using the low-pass filter, an inverse FFT transforms the frequency image back to the image domain. Random artifacts are uniformly distributed from the low to high frequency components of the frequency image (Hassan, 1988). Although FFT filtering cannot entirely remove these random artifacts, the artifacts at low frequencies will be dominated by more signal and/or information that is intrinsic to the image making the artifacts less recognizable.

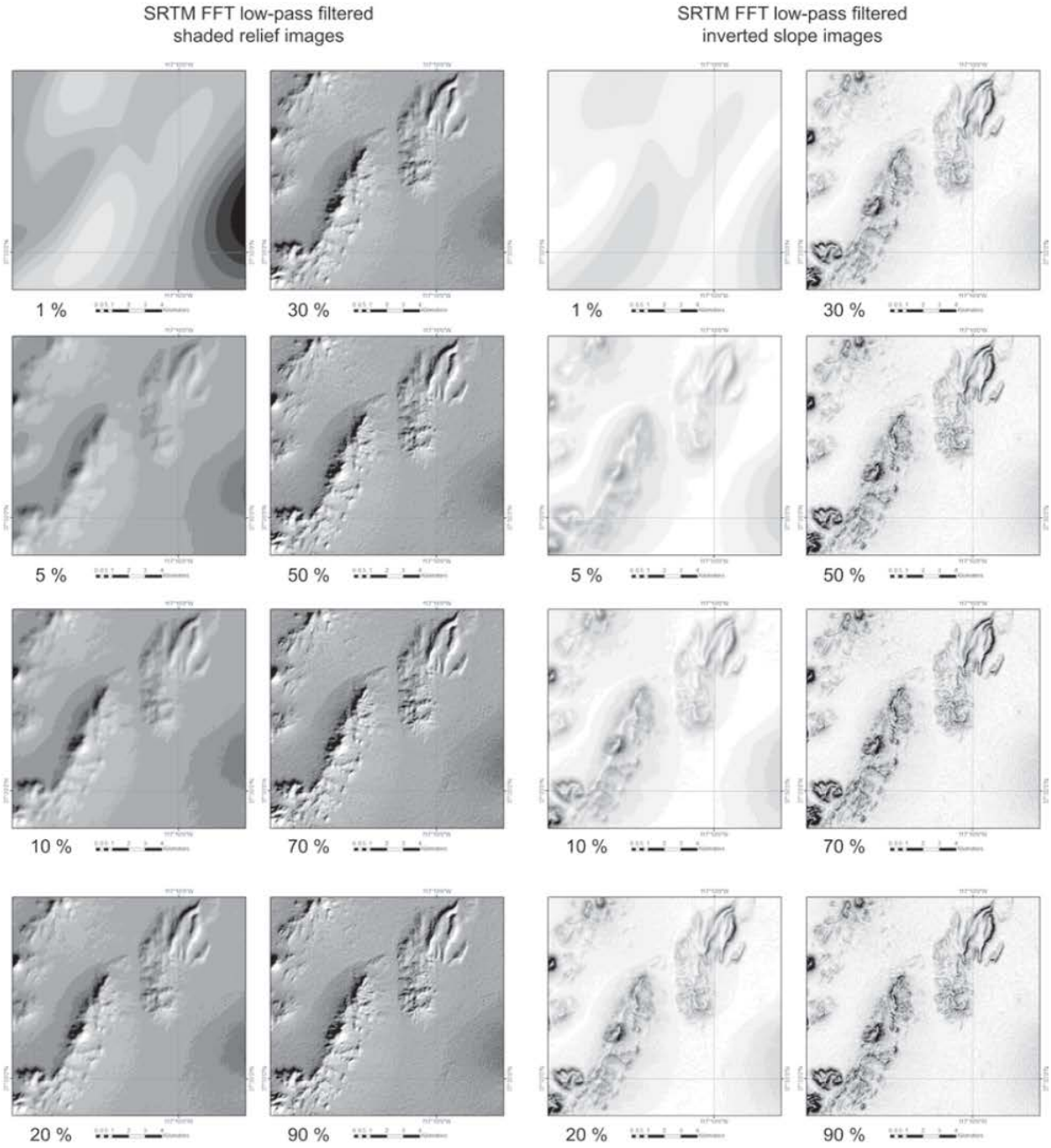

Figure 6: SRTM DEM FFT filtered shaded relief images and inverted slope images of different low-pass filter sizes

7. Discussion

Inverted slope images, such as that shown in Figure 2 (g), clearly show areas of outcrops and provide even more information of the differences in lithological units when compared to published geological maps (Figure 1). However, the inverted slope images created from image-derived DEMs (especially ASTER GDEM) are typically very noisy (Figure 2 (h), (i)). This happens because the image-derived DEM contains artifacts that do not reflect the true topography, especially since artifacts are frequently produced when DEMs are generated. While most of the artifacts in the original image-derived DEMs are difficult to recognize, they are typically exaggerated as noise in the inverted slope images. Detailed information of landforms and lithology is often hidden by this noise. ASTER GDEM is particularly noisy in low-relief areas because image correlation is more difficult to accomplish in images of flat terrains (Fujisada et al., 2005). Reducing artifacts from ASTER GDEM is essential because, compared to NED and SRTM DEM, more noise appears in inverted slope images produced from ASTER GDEM data. FFT transforms the DEM data into the frequency domain, with a range of high to low frequency components. Although it is possible to filter specific frequencies from the FFT frequency image, excessive filtering will remove original topographic information. The optimum filter size is thus one that minimizes the loss of topographic information while maximizing the removal of artifacts. An exponential circle filter was used for low-pass filtering because an ideal circle filter truncates the cutoff frequency and produces ripple like phenomena (Oppenheim and Schafer, 1975). FFT frequency filtering at twelve low-pass filter sizes (1 %, 5 %, 10 %, 20 %, 30 %, 40 %, 50 %, 60 %, 70 %, 80 %, 90 %, 100 %) was applied to the original SRTM DEM and ASTER GDEM data (Figure 5 (c)). Using a small low-pass filter size maintains the very lowest frequency components and removes the large residue associated with the higher frequencies (Figure 5 (d)). Shaded and inverted slope images produced using FFT-filtered SRTM DEM data (Figure 6) and FFT-filtered ASTER GDEM data (Figure 7). It was found that the amount of noise in the images decreased with the size of the low-pass filter, but the spatial resolution of the images also decreased and the image became smoother. Changes in noise and terrain resolution associated with FFT filtering were more apparent in inverted slope images than in shaded relief images. In order to determine optimum filter size, the differences between mean NED DEM, FFT-filtered SRTM DEM and ASTER GDEM values at different low-pass filter sizes was computed and plotted in Figure 8. A specific filter showing the minimum artifact size relative to the most topographic information for the filtered DEM was not obtained, but a trend approximating the optimal filter size was clarified. As the size of the low-pass filter was decreased, the number of artifacts in the DEM was reduced, but, as a tradeoff, some of the original topographic information was also lost. For both SRTM DEM and ASTER GDEM data, artifact reduction was constant when the low-pass filter size exceeded 40 %; at filter sizes of less than 20 %, the loss of artifact and topographic information increased. Thus, a filter size of 20 to 40 % was considered optimal for maximizing artifact reduction while reducing the loss of topographic information in this study. No significant difference was observed in assessments of optimum filter size in both SRTM DEM and ASTER GDEM data. Topographic and slope sections of FFT-filtered SRTM DEM and ASTER GDEM data transformed using a filter size of 30 % are shown in Figure 9. Random artifacts present in the original SRTM DEM and ASTER GDEM data (Figure 3 (b), (c)) were generally reduced (Figure 9 (a), (b)), but the DEM artifacts associated with cloud occurrence in the GDEM data persisted in the flat areas. These single-spike errors need to be removed by selective spatial filtering. The slope sections obtained from the original SRTM DEM and ASTER GDEM data could not be interpreted as being the same terrain (Figure 3 (e), (f)). However, when the same slope sections of SRTM DEM and ASTER GDEM data were transformed using a filter size of 30 %, the resulting topology was comparable with the same areas in the NED DEM images (Figure 3 (d), Figure 9 (c), (d)).

8. Conclusions

Inverted slope images show differences in lithology more clearly than images of the same areas showing only the shaded relief. While inverted images are useful for geological mapping, artifacts in the image-derived DEM data give the images a noisy texture and obscure information related to lithological units. Although the artifacts in the SRTM DEM and ASTER GDEM data are typically minor and unrecognizable in the original topographic data, they become exaggerated in the inverted slope images and produce images with a noisy texture. We attempted to reduce the artifacts in image-derived DEMs by FFT filtering and successfully removed high to medium-low frequency artifacts in the frequency image.

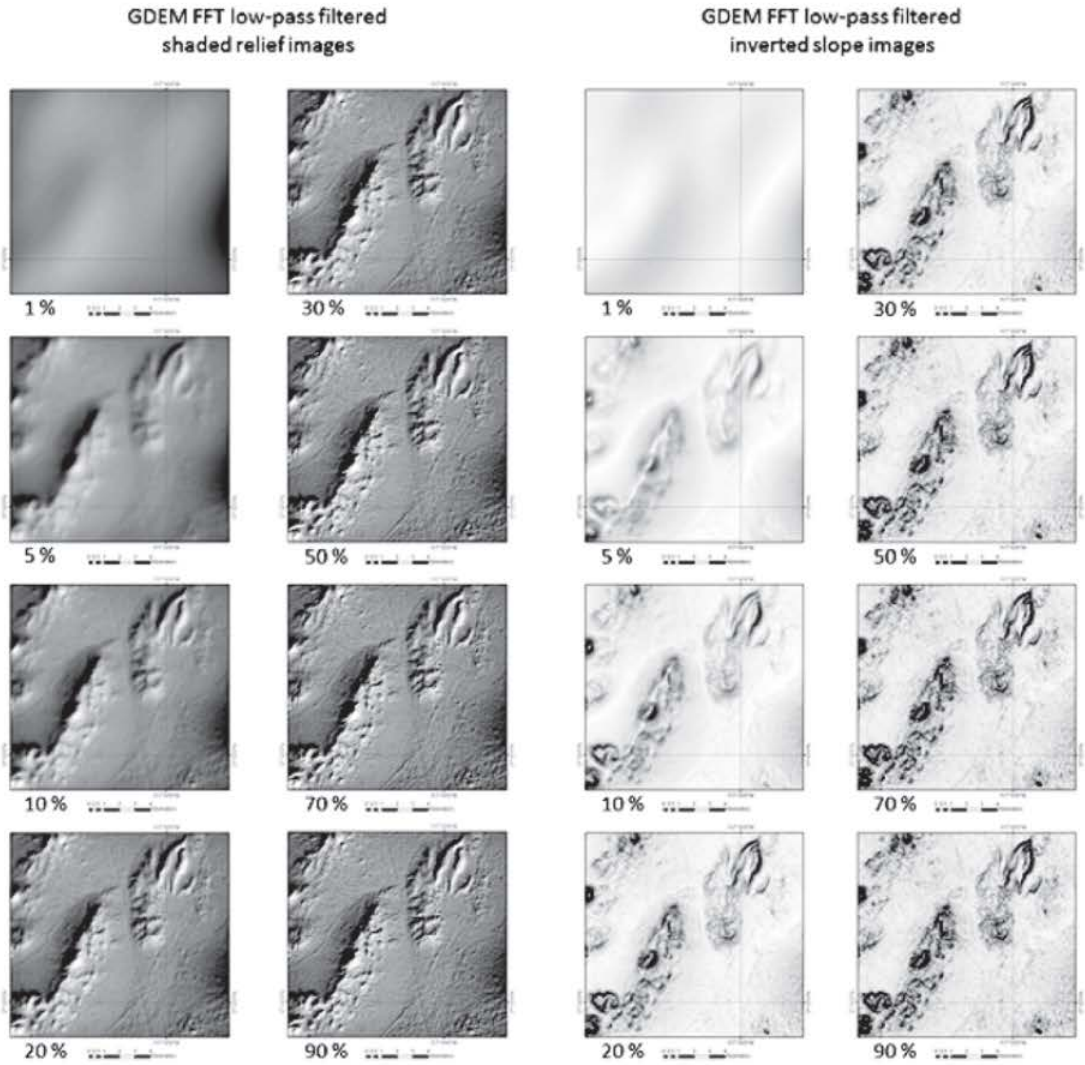

Figure 7: GDEM FFT filtered shaded relief images and inverted slope images of different low-pass filter sizes

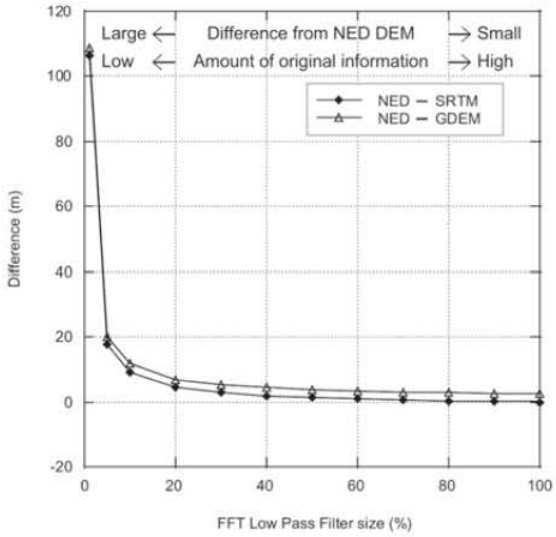

Figure 8: Difference of mean values between NED DEM and FFT filtered image derived DEM data at various low-pass filter sizes

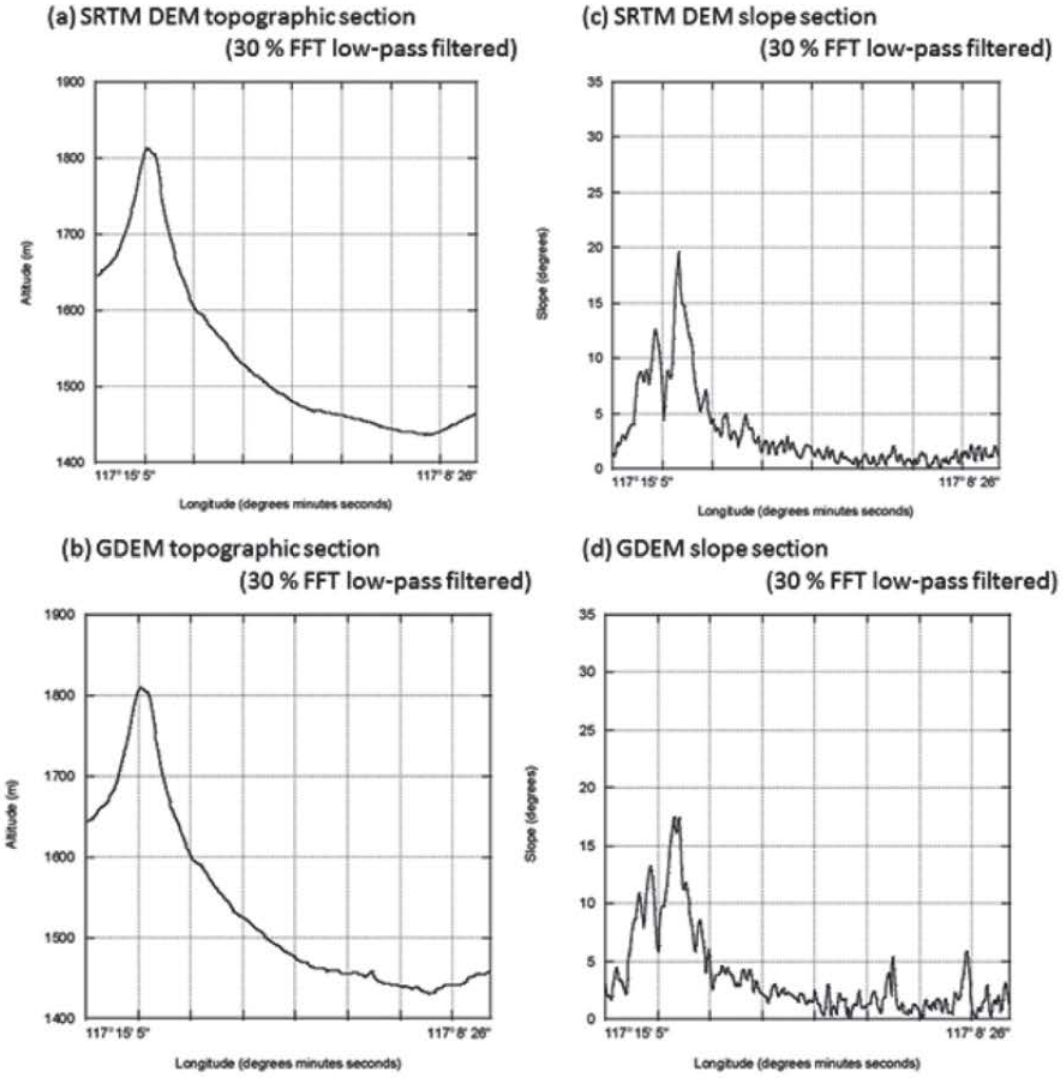

Figure 9 Topographic section and slope section of 30 % FFT low-pass filtered DEM

Specifically, low-pass filtering using an exponential circle filter with a size of 20 to 40 % effectively reduced the artifacts without a significant loss of terrain information from the image-derived DEMs in the study area. Compared to SRTM DEM, inverted ASTER GDEM images of flat terrain had high levels of noise which obscured the underlying topographical information. It is therefore necessary to reduce artifacts from ASTER GDEM data before creating shaded relief or slope images. Inverted slope images created from artifact-reduced DEM data subjected to FFT filtering can facilitate the accurate classification of lithological variation and rock composition.

References

Albani, M. and Klinkenberg, B., 2003, A Spatial Filter for the Removal of Striping Artifacts in Digital Elevation Models. *Photogrammetric Engineering & Remote Sensing*, 69, 755–765.

Badura, J. and Przybylski, B., 2005, Application of Digital Elevation Models to Geological and Geomorphological Studies – Some Examples. *Przegląd Geologiczny*, 53(10), 977-983.

Brown, D. G. and Bara, T. J., 1994, Recognition and Reduction of Systematic Error in Elevation and Derivative Surfaces from 7.5-minute DEMs. *Photogrammetric Engineering and Remote Sensing*, 60, 189-194.

Crafford, A. E. J., 2007, Geologic Map of Nevada. *U.S. Geological Survey Data Series 249*, 46.

Crosta, A. P. and Moore, J. McM., 1989, Enhancement of Landsat Thematic Mapper Imagery for Residual Soil Mapping in SW Minas Gerais State Brazil: A Prospecting Case History in Greenstone Belt Terrain. *Proceedings of the 9th Thematic Conference on Remote Sensing for Exploration Geology, Calgary* (Ann Arbor, MI: Environmental Research Institute of Michigan), 1173-1187.

De Souza Filho, C. R., Drury, S. A., Denniss, A. M., Carlton, R. W. T., and Rothery, D. A., 1996, Restoration of Corrupted Optical Fuyo-1 (JERS-1) Data using Frequency Domain Techniques. *Photogrammetric Engineering and Remote Sensing*, 62, 1037-1047.

Fujisada, H., Bailey, G. B., and Kelly, G. G., 2005, ASTER DEM Performance. *IEEE Transactions on Geoscience and Remote Sensing*, 43, 2707-2714.

Gesch, D. B., Muller, J. P., and Farr, T. G., 2006, The Shuttle Radar Topography Mission – Data Validation and Applications. *Photogrammetric Engineering and Remote Sensing*, 72, 233-235.

Green, A. A., Berman, M., Switzer, P. and Craig, M. D., 1988, A Transformation for Ordering Multispectral Data in Terms of Image Quality with Implications for Noise Removal. *IEEE Transactions on Geoscience and Remote Sensing*, 26, 65-74.

Guth, P. L., 1999, Contour Line "Ghosts" in USGS Level 2 DEMs. *Photogrammetric Engineering and Remote Sensing*, 65, 289-296.

Guth, P. L., 1995, Slope and Aspect Calculations on Gridded Digital Elevation Models: Examples from a Geomorphometric Toolbox for Personal Computers. *Zeitschrift fir Geomorphologie*, 101, 31-52.

Hassan, M. M., 1988, Filtering Digital Profile Observations, Photogrammetric Engineering and Remote Sensing, 54 (10), 1391-1394.

Hewson, R. D., Cudahy, T. J., Mizuhiko, S., Ueda, K. and Mauger, A. J., 2005, Seamless Geological Map Generation using ASTER in the Broken Hill–Curnamona Province of Australia. *Remote Sensing of Environment*, 99, 159–172.

Iwahashi, J. and Pike, R. J., 2007, Automated Classifications of Topography from DEMs by an Unsupervised Nested-Means Algorithm and a Three-Part Geometric Signature. *Geomorphology*, 86, 409-440.

Kruse, F. A., 2002, Comparison of AVIRIS and Hyperion for Hyperspectral Mineral Mapping. 11th JPL Airborne Geoscience Workshop.

Kruse, F. A., Boardman, J. W., and Huntington, J. F., 2003, Comparison of Airborne Hyperspectral Data and EO-1 Hyperion for Mineral Mapping. *IEEE Transactions on Geoscience and Remote Sensing*. 41, 1388-1400.

Loughlin, W. P., 1991, Principal Component Analysis for Alteration Mapping. *Photogrammetric Engineering and Remote Sensing*, 57, 1163-1169.

Masoud, A. and Koike, K., 2006, Tectonic Architecture through Landsat-7 ETM+/SRTM DEM-Derived Lineaments and Relationship to the Hydrogeologic Setting in Siwa Region, NW Egypt. *Journal of African Earth Sciences*, 45, 467-477.

Oppenheim, A. V. and Schafer, R. W., 1975, Digital Signal Processing. Prentice-Hall, 585.

Pan, J. J., 1989, Spectral Analysis and Filtering Techniques in Digital Spatial Data Processing. *Photogrammetric Engineering and Remote Sensing*, 55, 1203-1207.

Rabus, B, Eineder, M. and Roth, A., 2003, The Shuttle Radar Topography Mission - a New Class of Digital Elevation Models Acquired by Spaceborne Radar. *ISPRS Journal of Photogrammetry and Remote Sensing*, 57, 241-262.

Rowan, L. C., Hook, S. J., Abrams, M. J., and Mars, J. C., 2003, Mapping Hydrothermally Altered Rocks at Cuprite, Nevada, using the Advanced Spaceborne Thermal Emission and Reflection Radiometer (ASTER), A New Satellite-Imaging System. *Economic Geology*, 98, 1019-1027.

Singh, B. and Dowerah, J., 2010, ASTER DEM Based Studies for Geological Investigation around Singhbhum Shear Zone (SSZ) in Jharkhand, India. *Journal of Geographic Information System*, 2, 11-14.

Smith, M. J. and Clark, C. D., 2005, Methods for the Visualization of Digital Elevation Models for Landform Mapping. *Earth Surface Processes and Landforms*, 30, 885–900.

Tachikawa, T., Hato, M., Kaku, M., and Iwasaki, A., 2011, The Characteristics of ASTER GDEM Version 2. *IGARSS 2011 Vancouver*, 3657-3661.